PHYSICAL REVIEW B VOLUME 24, NUMBER 4 15 AUGUST 1981

Interband magnetoabsorption in semimagnetic semiconductor alloys $Hg_{1-k}Mn_kTe$ with a positive energy gap

G. Bastard, C. Rigaux, and Y. Guldner
Groupe de Physique des Solides de l'Ecole Normale Superieure, 24 rue Lhomond, 75231 Paris Cedex 05, France*

A. Mycielski
Institute of Physics, Polish Academy of Sciences, 02-668 Warsaw, Poland

J. K. Furdyna and D. P. Mullin†
Department of Physics, Purdue University, West Lafayette, Indiana 47907
(Received 2 March 1981)

Low-temperature infrared magnetoabsorption experiments were carried out on $Hg_{1-k}Mn_kTe$ mixed crystals with compositions corresponding to the semiconducting (positive energy gap) range. Measurements were performed in the spectral region 100–350 meV in Voigt and Faraday geometries, using both linear and circular polarizations. The magneto-optical data provide observation of interband $\Gamma_8 \rightarrow \Gamma_6$ transitions. In addition, transitions from acceptor levels to Γ_6 Landau levels were observed. The interband magneto-optical transitions are interpreted within the framework of the Pidgeon-Brown model, modified by the contributions of the *s-d* and *p-d* spin-spin exchange interaction between band electrons and localized Mn^{2+} spins. From the theoretical fits of the transition energies to the observed absorption lines, the relative magnetization $A(H,T)$ is deduced at $T = 4.2$ and 2 K for alloys of various Mn content. In contrast with zero-gap $Hg_{1-k}Mn_kTe$, in the present case $A(H,T)$ exhibits a nearly linear magnetic field dependence and depends only weakly on temperature. These features are related to the strong antiferromagnetic interactions between the localized magnetic moments. Conduction electrons in crystals in this composition range exhibit large and *positive* g factors as a consequence of the *s-d* exchange coupling.

I. INTRODUCTION

Magneto-optical studies in semimagnetic semiconductors[1–5] have emphasized the strong influence of spin-spin exchange interaction between localized magnetic moments and band electrons on the spin splitting of Landau levels in these materials. Previous experiments, performed on zero-gap $Hg_{1-k}Mn_kTe$ alloys[2] have shown a dramatic enhancement of the gyromagnetic factors for electronic levels in both Γ_6 and Γ_8 bands as a result of this exchange interaction. These g factors were observed to depend strongly on temperature. Moreover, exchange interactions between d electrons and band electrons were shown to induce a significant shift of the uppermost valence level, leading to new striking features in magneto-optical[2] and magneto-transport[6] phenomena.

To facilitate discussion, the energy-band structure of $Hg_{1-k}Mn_kTe$ at the center of the Brillouin zone (the Γ point) is shown schematically for various compositions in Fig. 1. The effect of spin-spin ex-

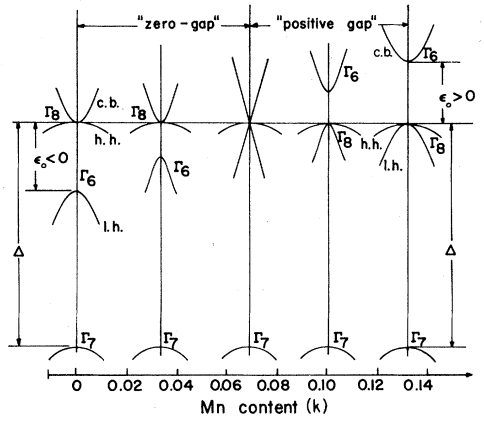

FIG. 1. The energy-band structure of $Hg_{1-k}Mn_kTe$ at the center of the Brillouin zone (the Γ-point) for various compositions of the alloy. In the "zero-gap" region ($k < 0.07$), ϵ_0 is negative. The positive-gap ($\epsilon_0 > 0$) region, of interest in this paper, begins at $k > 0.07$ for liquid helium temperatures. The labels "*c.b.*," "*h.h.*," and "*l.h.*" indicate the conduction band and heavy- and light-hole bands, respectively.

change on Landau levels in zero-gap $Hg_{1-k}Mn_kTe$ mixed crystals ($k < 0.07$) has been understood by incorporating the *s-d* and *p-d* exchange contributions between the band electrons and the localized Mn^{2+} moments, formulated in terms of the molecular-field approximation, into the framework of the Pidgeon-Brown model.[7] It was particularly interesting to extend magneto-optical studies to $Hg_{1-k}Mn_kTe$ alloys in the semiconducting (positive energy gap) range, which correspond to a significantly larger value of k than the zero-gap crystals (see Fig. 1), and for which important exchange effects were therefore expected due to the large concentration of the manganese ions.

We have investigated $Hg_{1-k}Mn_kTe$ alloys with Mn content-ranging from 0.1 to 0.2, using low-temperature magnetoabsorption carried out in the spectral region between 100 and 350 meV. We report the salient features of magneto-optical spectra corresponding to interband transitions from Γ_8 to Γ_6 bands, with emphasis on the effects induced by the spin-spin exchange phenomena. In contrast with zero-gap materials, the magneto-optical spectra are only weakly dependent on temperature between 4.2 and 2 K, reflecting a small variation of the magnetization in this temperature range.

Remarkable peculiarities originating from exchange effects on Γ_8 and Γ_6 Landau levels are observed. These include a reduction of the energy gap in applied magnetic field and the inversion of the ordering of "electron-spin-up" and "electron-spin-down" sublevels, leading to positive gyromagnetic factors for the conduction electrons. Magnetoabsorption spectra for semiconducting alloy compositions with $k \simeq 0.13-0.15$ also systematically show certain anomalies which are related to the interference of acceptor-to-Γ_6 transitions with interband $\Gamma_8 \rightarrow \Gamma_6$ transitions.

II. EXPERIMENTAL PROCEDURE

Single crystals of $Hg_{1-k}Mn_kTe$ were grown by a modified Bridgman method, providing ingots of high homogeneity. The Mn molar content was determined for all investigated samples by density measurements. In addition, electron microprobe analysis was also performed on several samples. Samples were prepared by cutting slices from the Bridgman ingots, which were then mechanically polished and annealed under a saturated atmosphere of mercury for a period of 100–200 h to reduce the density of mercury vacancies. The samples used for transmission measurements were finally prepared by etching the annealed slices in bromine-methanol solution to a thickness of several micrometers.

Magnetotransmission spectra were obtained at 4.2 and 2 K by sweeping the magnetic field (up to 60 kG) at fixed infrared photon energies, in the spectral region from 100 to 350 meV. Some magnetoabsorption lines were also obtained by sweeping the photon energy at fixed values of the magnetic field. This procedure was the most effective for observing transitions whose energies vary slowly with magnetic field (i.e., lines labeled 0 in Figs. 4–7). Magnetoabsorption spectra were observed either in the Voigt geometry using incident linear polarization ($\hat{\epsilon} \,||\, \vec{H} \,||\, \hat{z}$), or in the Faraday geometry using incident left- and right-handed circular polarizations (labeled in the text as σ^+ and σ^-, respectively), to select the magneto-optical transitions induced by each radiation polarization with $\hat{\epsilon}_{||} = \hat{z}$, $\hat{\epsilon}^+ = (\hat{x} + i\hat{y})/\sqrt{2}$, and $\hat{\epsilon}^- = (\hat{x} - i\hat{y})/\sqrt{2}$, respectively, where $\hat{\epsilon}$ indicates the unit vector parallel to the electric field of the incident wave.

III. EXPERIMENTAL RESULTS

In Fig. 2 we present examples of magnetotransmission spectra obtained at fixed photon energies, for different incident polarizations. For the lowest-energy transition, the relative transmission

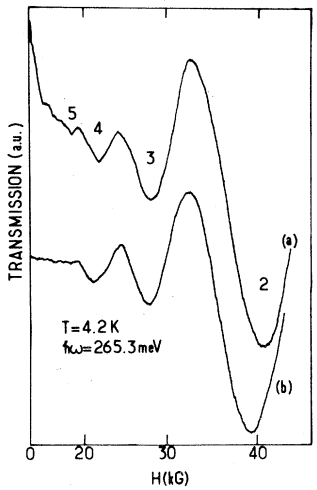

FIG. 2. Magnetotransmission spectra for σ^- and $\hat{\epsilon} \,||\, \vec{H}$ polarizations labeled "*a*" and "*b*", respectively, observed at the photon energy $\hbar\omega = 265.3$ meV at $T = 4.2$ K for an alloy with $k = 12.8$ at. %. Individual transitions are identified by the corresponding quantum number n according to Eqs. (12) and (13).

$[T(H) - T(0)]/T(0)$ at various fields is also plotted in Fig. 3 as a function of the photon energy, as described earlier. Photon energies corresponding to the observed transmission minima are plotted as a function of magnetic field in Figs. 4–7, for $\hat{\epsilon} \,||\, \vec{H}$ and σ^- polarization, for alloys of various Mn content. In these plots, the extrapolation of the energies of the magnetoabsorption lines to vanishing magnetic fields converges to the value of the energy gap $\epsilon_0 = E_{\Gamma_6} - E_{\Gamma_8}$.

The polarization and temperature dependence of the observed spectra reveal the following characteristic features which contrast with the behavior of interband magnetotransmission observed in other materials:

1. Except for the two lowest-energy transitions [lines labeled 0 and 1 in Figs. 4(a), 4(b) and 4(c), 4(d)], the lines observed for $\hat{\epsilon} \,||\, \vec{H}$ and σ^- polarization are nearly in coincidence [lines 2,3,4. . . in Figs. 4(a), 4(b) and 4(c), 4(d)]. This feature is also evident from Fig. 2, which shows examples of magnetotransmission spectra for $\hat{\epsilon} \,||\, \vec{H}$ and σ^- polarizations observed at $\hbar\omega = 265.3$ meV for an alloy of $k \simeq 12.8$ at. %. This behavior was systematically seen in all samples in the present investigation, and contrasts with results obtained on zero-gap $Hg_{1-k}Mn_kTe$.

2. For σ^+ polarization, only very weak structures are observed in the magnetotransmission high-energy region, in sharp contrast with the pronounced transmission minima of the σ^- and $\hat{\epsilon} \,||\, \vec{H}$ spectra.

3. On decreasing temperature from 4.2 to 2 K, the energies of the two lowest transitions (lines 0 and 1 in both $\hat{\epsilon} \,||\, \vec{H}$ and σ^- spectra) are shifted downwards, whereas the positions of the other resonant lines are practically unmodified, again in contrast with zero-gap $Hg_{1-k}Mn_kTe$, where high-energy transitions also show noticeable temperature dependence due to the exchange interaction.

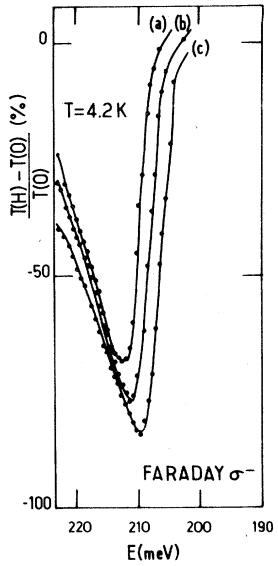

FIG. 3. Relative transmission $[T(H) - T(0)]/T(0)$ at three different magnetic fields, observed with the σ^- polarization as a function of photon energy at $T = 4.2$ K, for $k = 12.8$ at. %. Curve (a) corresponds to $H = 23.6$ kG, (b) to $H = 33.1$ kG, and (c) to $H = 51.7$ kG. The minimum of each curve corresponds to the lowest-energy transition [$n = 0$ in Eq. (13)].

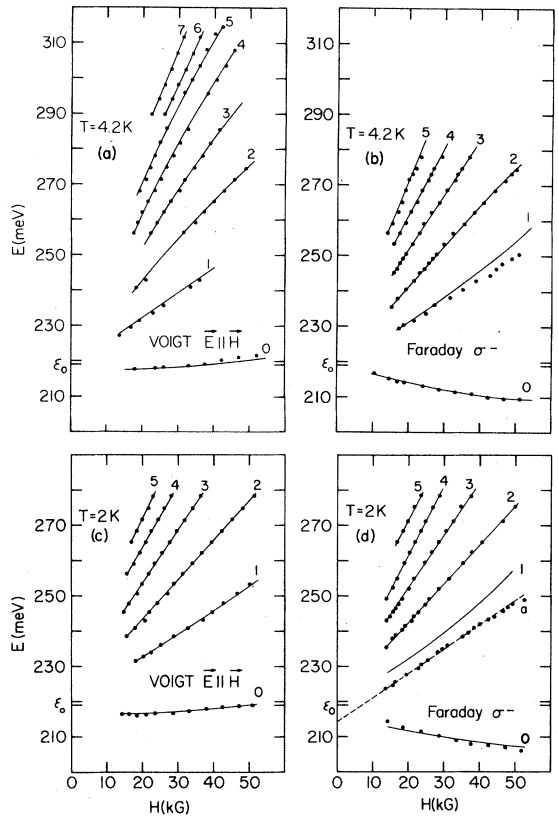

FIG. 4. Energies of successive transmission minima vs magnetic field for an alloy with $\epsilon_0 = 219$ meV ($k = 12.8$ at. %) for temperatures and configurations indicated in the figure. Points are experimental; solid lines represent theoretical fits with the modified Pidgeon-Brown model. The quantum number n identifying the transitions according to Eqs. (12) and (13) is shown for each curve. Note that in Fig. 4(d) the line labeled α lies significantly below the $n = 1$ curve and does not extrapolate to ϵ_0.

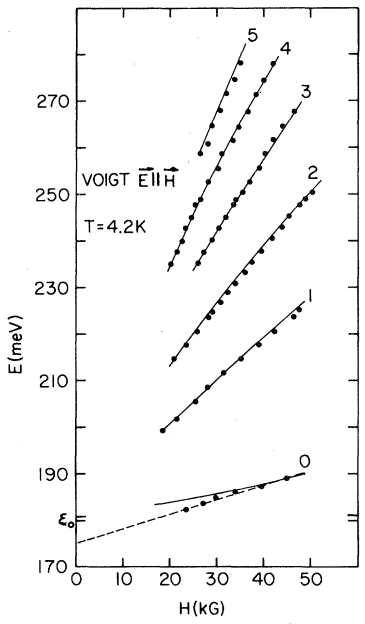

FIG. 5. Energies of transmission minima *versus* magnetic field for an alloy with $\epsilon_0 = 181$ meV, for the $\hat{\epsilon} \| \vec{H}$ polarization at 4.2 K. Points are experimental; solid lines are theoretical fits. Quantum numbers n identifying the transitions according to Eq. (12) are indicated for each line.

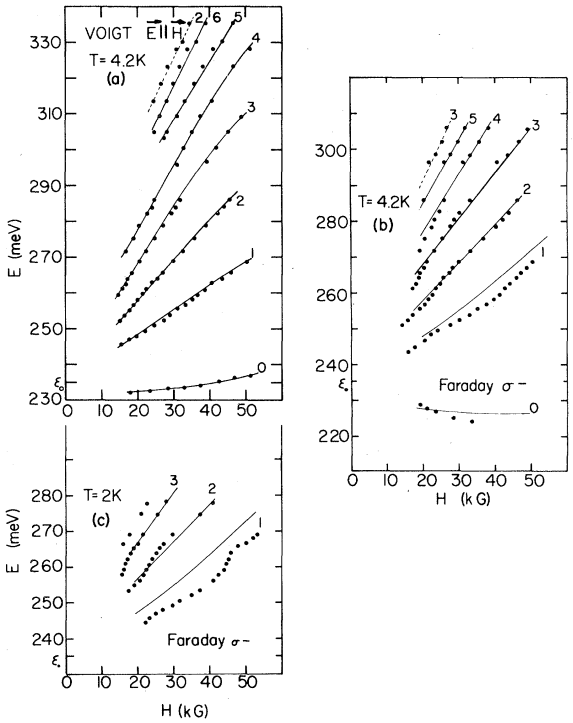

FIG. 6. Energies of transmission minima *versus* magnetic field for an alloy with $\epsilon_0 = 235$ meV for temperatures and configurations indicated in the figure. Points are experimental; solid curves are theoretical fits, with n identifying successive transitions indicated for each curve according to Eqs. (12) and (13). The dashed curves in Figs. 6(a) and 6(b) represent calculated energies for light-hole transitions [$n = 2$ in Eq. (12) for (a); $n = 3$ in Eq. (13) for (b)].

IV. THEORETICAL ANALYSIS AND DISCUSSION OF RESULTS

A. Landau levels at the Γ point

The interpretation of the magneto-optical data was made by using a modified Pidgeon-Brown model[7,8] which provides the magnetic field dependence of Landau levels for the Γ_6 and Γ_8 bands. The modifications of the Pidgeon-Brown model consists of incorporating into the model contributions of *s-d* and *p-d* interactions of the band electrons with localized magnetic moments, formulated in terms of the molecular-field approximation.[2,6]

The magnetic energy levels at the Γ point are obtained by solving an 8×8 matrix Hamiltonian. When inversion asymmetry and warping of the Γ_8 bands is neglected, the 8×8 Hamiltonian D simplifies into two decoupled 4×4 matrices $\bar{D}_a$ and $\bar{D}_b$,

$$D = \left[\begin{array}{c:c} \bar{D}_a & 0 \\ \hdashline 0 & \bar{D}_b \end{array}\right], \qquad (1)$$

written in the basis of the eight band-edge Bloch u_{J,m_J} functions, as given in Refs. (7) and (8). The 4×4 matrices in Eq. (1) can be written

$$\bar{D}_a = D_a + M_a \ , \qquad (2)$$

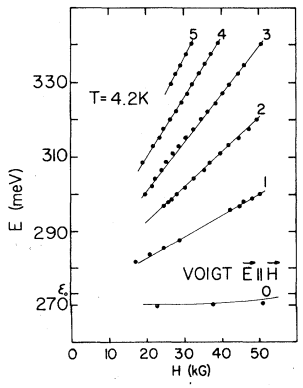

FIG. 7. Energies of transmission minima *versus* magnetic field for an alloy with $\epsilon_0 = 273$ meV for the $\hat{\epsilon} \| \vec{H}$ polarization at 4.2 K. Points are experimental; solid curves are theoretical fits, with n for each transition indicated according to Eq. (12).

$$\bar{D}_b = D_b + M_b \ , \tag{3}$$

where D_a and D_b are the matrix Hamiltonians of the unmodified Pidgeon-Brown model,[7,8] i.e., without exchange interaction. The contribution of the exchange interaction is introduced through matrices M_a,M_b, in the form[2]

$$M_a = \begin{bmatrix} 3Ar & 0 & 0 & 0 \\ 0 & 3A & 0 & 0 \\ 0 & 0 & -A & -2A\sqrt{2} \\ 0 & 0 & -2A\sqrt{2} & A \end{bmatrix} , \tag{4}$$

$$M_b = \begin{bmatrix} -3Ar & 0 & 0 & 0 \\ 0 & A & 0 & 2A\sqrt{2} \\ 0 & 0 & -3A & 0 \\ 0 & 2A\sqrt{2} & 0 & -A \end{bmatrix} , \tag{5}$$

where $r = \alpha/\beta$ is the ratio between the Γ_6 exchange integral $\alpha = \langle S \,|\, J(\vec{r}) \,|\, S \rangle$ and the Γ_8 exchange integral $\beta = \langle X \,|\, J(\vec{r}) \,|\, X \rangle$, and A is the normalized magnetization parameter

$$A = \tfrac{1}{6}\beta k N_0 \langle S_z \rangle \ . \tag{6}$$

Here N_0 is the number of unit cells per unit volume of the crystal, k is the molar fraction of Mn in the alloy, and $\langle S_z \rangle$ is the thermal average of the spin operator along the direction of the applied magnetic field. The average $\langle S_z \rangle$ depends on the field H and temperature T as

$$\langle S_z \rangle = -S f_{\text{norm}}(H,T) \ , \tag{7}$$

where $S = \frac{5}{2}$ is the spin of the Mn^{2+} ion and f_{norm} is a normalization function such that

$$f_{\text{norm}}(0,T) = 0 < f_{\text{norm}}(H,T) < f_{\text{norm}}(\infty,T) = 1 \ . \tag{8}$$

For very small values of k (noninteracting Mn^{2+} spins) f_{norm} can be expressed as

$$f_{\text{norm}}(H,T) = \tfrac{2}{5} B_{5/2}\left[\frac{g_{\text{Mn}}\mu_B H}{k_B T}\right] , \tag{9}$$

where $B_{5/2}$ is the Brillouin function for spin $\frac{5}{2}$, with g_{Mn} the g factor of the Mn^{2+} ion, μ_B the Bohr magneton, and k_B the Boltzmann constant. For the present case of relatively concentrated Mn content, this relationship can no longer be quantitatively applied. It can, however, provide a phenomenological description of magnetization $A(H,T)$ in more concentrated spin systems if T in Eq. (9) is replaced by an empirical temperature parameter $T + T_{\text{eff}} > T$.

It is an important feature of the above formulation that the eigenstates of $\bar{D}_a$ and $\bar{D}_b$ have the same form as those of D_a and D_b, respectively. As in the case of the unmodified Pidgeon-Brown model, one then obtains the eigenvalues and eigenfunctions for the magnetic sublevels by numerically solving the two decoupled eigenvalue equations,

$$(\bar{D}_a - E_a I)\begin{bmatrix} f_1 \\ f_3 \\ f_5 \\ f_7 \end{bmatrix} = 0 \tag{10}$$

and

$$(\bar{D}_b - E_b I)\begin{bmatrix} f_2 \\ f_4 \\ f_6 \\ f_8 \end{bmatrix} = 0 \ , \tag{11}$$

where $f_i (i = 1 \ldots 8)$ are appropriate envelope functions, which in this case can be expressed in terms of the harmonic oscillator functions.[7,8] The physical distinction between the two sets of solutions is that, in the case of conduction electrons in the parabolic limit $[E_a(n),E_b(n) << \epsilon_0]$, the a set corresponds to $\sigma_z = \frac{1}{2}$ spin sublevels ("spin up") and the b set to $\sigma_z = -\frac{1}{2}$ spin sublevels ("spin down"). The parameters of the model are the following: the energy gap $\epsilon_0 = E_{\Gamma_6} - E_{\Gamma_8}$, the spin-orbit splitting $\Delta = \Gamma_8 - \Gamma_7$, the Kane matrix element for the interaction between s and p bands $E_p = (2/m_0)\,|\langle S \,|\, p_x \,|\, X \rangle|^2$, the modified Luttinger parameters γ_1, $\bar{\gamma}$, and κ, as well as the parameters of exchange interaction A and r. For further details of the model, including explicit analytic expressions for the wave functions, the reader is referred to Refs. 2 and 8.

B. Interband transitions and selection rules

The selection rules for the Γ_8-to-Γ_6 transitions are the same as those established for nonmagnetic systems.[8] They are summarized in Table I. In the table, σ^+ and σ^- refer, respectively, to the two senses of circular polarization of waves incident in the Faraday geometry, $\hat{\epsilon} \,||\, \vec{H}$ corresponds to the linear polarization in the Voigt geometry, and n is the Landau-level quantum number.

Quantitative analysis of the transition probabilities (which are dependent on the exchange contribution) indicates that the transitions originating from heavy-hole Landau levels should be much weaker

TABLE I. Selection rules for the Γ_8-to-Γ_6 transitions.

Polarization	Allowed transitions
σ^+	$a_{\Gamma_8}(n)\rightarrow a_{\Gamma_6}(n+1)$, $b_{\Gamma_8}(n)\rightarrow b_{\Gamma_6}(n-1)$
σ^-	$a_{\Gamma_8}(n)\rightarrow a_{\Gamma_6}(n+1)$, $b_{\Gamma_8}(n)\rightarrow b_{\Gamma_6}(n+1)$
$\hat{\epsilon}\,\|\|\,\vec{H}$	$a_{\Gamma_8}(n-1)\rightarrow b_{\Gamma_6}(n)$, $b_{\Gamma_8}(n+1)\rightarrow a_{\Gamma_6}(n)$

for σ^+ than for the σ^- and $\hat{\epsilon}\,\|\,\vec{H}$ polarizations.[9] For $\hat{\epsilon}\,\|\,\vec{H}$, transitions from heavy holes are the most intense, the dominant series of transitions corresponding to

$$a_{\Gamma_8}(n-1)\rightarrow b_{\Gamma_6}(n),\quad n\geq 0\ . \tag{12}$$

For the σ^- polarization, on the other hand, transitions involving both heavy and light holes are expected to be strong, with the dominant series corresponding to

$$b_{\Gamma_8}(n-1)\rightarrow b_{\Gamma_6}(n),\quad n\geq 0\ . \tag{13}$$

The most prominent lines of the spectra correspond to $n=0$ and $n=+1$ in Eqs. (12) and (13) and should be observed for both σ^- and $\hat{\epsilon}\,\|\,\vec{H}$ polarizations. In the case of the lowest-energy transitions one should expect pronounced exchange effects, particularly for $b_{\Gamma_8}(-1)\rightarrow b_{\Gamma_6}(0)$, due to the large exchange-induced shift $\Delta E_b(-1)=-3A$ experienced by the heavy-hole Landau level $b_{\Gamma_8}(-1)$.

The experimental lines observed for the $\hat{\epsilon}\,\|\,\vec{H}$ and σ^- polarizations are identified in Figs. 4–7 according to the selection rules (12) and (13), with the quantum number n corresponding to each transition indicated in the figures. The fact that the energy levels $a_{\Gamma_8}(n-1)$ and $b_{\Gamma_8}(n-1)$ for heavy holes lie very close together explains the near coincidence of the lines observed for σ^- and $\hat{\epsilon}\,\|\,\vec{H}$ polarizations for $n\geq 2$.

A quantitative interpretation of the spectra was obtained by a least-squares fitting of the transition energies to the experimental lines. The parameters of the fitting procedure were restricted to the exchange parameters r and $A(H,T)$, and to the matrix element $E_p=2|\langle S|p_x|X\rangle|^2/m_0$. The remaining band parameters were taken to be equal to the values previously obtained for zero-gap $Hg_{1-k}Mn_kTe$ alloys.[2] The spin-orbit splitting is taken to be $\Delta=1$ eV, and the higher band parameters are fixed at the following values: $\gamma_1=3$, $\bar{\gamma}=0.05$, and $\kappa=-1.65$. The energy gap ϵ_0 is first approximately determined from the extrapolated energy of the transitions to zero magnetic field, and then adjusted to obtain the best theoretical fit of the spectra.

The comparison between theory and experiment is illustrated in Figs. 4–7 for alloys of different composition at $T=4.2$ and 2 K. For each alloy, the same values of the parameters [except $A(H,T)$, which depends on field and temperature] describe quite well the experimental data for both temperatures for both $\hat{\epsilon}\,\|\,\vec{H}$ and σ^- polarizations. For $\hat{\epsilon}\,\|\,\vec{H}$, excellent agreement is found between theory and experiment at 4.2 and 2 K for all transitions. Most of these transitions originate from the heavy-hole Landau levels, as expected from the model. For σ^- polarization the fits are also good, with the exception of one line which we identify as an acceptor level-to-Γ_6 transition.

C. Acceptor transition

For all investigated samples the σ^- spectra show systematic discrepancies between the calculated energy of the $b_{\Gamma_8}(0)\rightarrow b_{\Gamma_6}(1)$ transition and the experimental position of the transmission minima [Figs. 4(b), 4(d); 6(b), 6(c)]. The experimental line, labeled α in Fig. 4(d), lies systematically below the expected position of the interband transition. Line α cannot be attributed to an interband transition, as the zero-field energy extrapolated for this transition is lower than the energy gap [Fig. 4(d)]. Note also that the magnetotransmission spectrum in this energy range, shown in Fig. 8, consists of a broad and asymmetrical band whose transmission minimum corresponds to line α. The asymmetrical line shape indicates the presence, at lower field $H<H_\alpha$, of a weaker but unresolved structure which could be as-

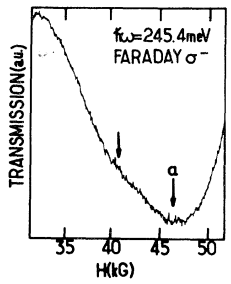

FIG. 8. Line shape of the magnetotransmission spectrum for the alloy with $\epsilon_0=219$ meV in the vicinity of the $n=1$ transition for the σ^- polarization at $T=2$ K, showing the acceptor (α) and interband transitions by arrows.

signed to the true interband $b_{\Gamma_8}(0) \rightarrow b_{\Gamma_6}(1)$ transition. We identify line α with a transition from an acceptor state to $b_{\Gamma_6}(1)$. In Fig. 9 we have plotted the energy of the acceptor level as a function of magnetic field, obtained from our experiments for the alloy with $\epsilon_0 = 219$ meV. In the plot, zero energy is taken at the top of the valence band (Γ point) at $H = 0$. The zero-field binding energy of the acceptor is estimated roughly as 5 ± 1 meV and the field dependence implies a decrease of the absolute value of the acceptor level in applied magnetic field.

The coexistence of both $\text{acc} \rightarrow b_{\Gamma_6}(1)$ and $b_{\Gamma_8}(0) \rightarrow b_{\Gamma_6}(1)$ transitions in the σ^- spectrum is further supported by the observation for some alloys of a gradual evolution of the transmission minima from the acceptor transition towards the interband transition as the magnetic field is increased. These features are shown on Fig. 6(c) for an alloy with $\epsilon_0 = 235$ meV. This peculiar behavior may be explained by the field dependence of the transition intensities I as the relative strengths corresponding to the two types of transitions exhibit opposite behavior: For $\text{acc} \rightarrow b_{\Gamma_6}(1)$ the intensity I_a is proportional to $N_a\lambda$, whereas for $b_{\Gamma_8}(0) \rightarrow b_{\Gamma_6}(1)$ the intensity I should vary as $1/\lambda^2$, where $\lambda^2 = hc/eH$ and N_a is the acceptor concentration.[10] With increasing magnetic field one thus expects a decrease of the strength of the acceptor transition I_a and an intensification of the interband transition. This may explain the observed energy shift of the transmission minima [Fig. 6(c)] even if both transitions coexist in the unresolved magnetotransmission spectrum. However, for most samples the density of acceptors was so high ($N_a \simeq 5 \times 10^{16}$ cm^{-3}) as to mask the observation of the interband transitions in the whole investigated field range, so that the dominant feature of the spectrum in this region was the acceptor transition. The presence of the $\text{acc} \rightarrow b_{\Gamma_6}(1)$ transition thus explains the systematic discrepancies between theory and experiment observed in the σ^- spectra for all samples.

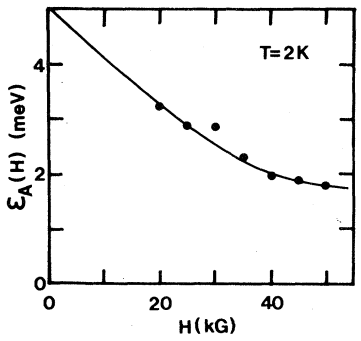

FIG. 9. Magnetic field dependence of the acceptor level obtained for the alloy with $\epsilon_0 = 219$ meV for $T = 2$ K. Zero energy is taken at the top of the valence band at $H = 0$. Note the dramatic decrease of ϵ_A as the field increases.

D. Material parameters obtained

Band and exchange parameters were determined from the theoretical fits of the $\Gamma_8 \rightarrow \Gamma_6$ transitions. Figure 10 shows the evolution of the interaction gap of $Hg_{1-k}Mn_kTe$ alloys as a function of Mn content, also including data for zero-gap semiconductors obtained earlier.[2] The interaction gap ϵ_0 exhibits a nonlinear variation as a function of composition k, changing the sign (zero-gap to positive-gap transition) for $k \simeq 7.4$ at. % at $T = 4.2$ K. The Kane matrix element shows a rather pronounced decrease with increasing Mn content, as shown in Fig. 11. This behavior contrasts with the results obtained for $Hg_{1-x}Cd_xTe$ alloys.[8,11] For the parameter r (ratio of the exchange integrals α/β), the best theoretical fits for alloys in the range of composition $0.12 < k < 0.17$ are achieved with $-0.9 \leq r \leq -0.7$. The relative magnetization $A(H,T)$ deduced from the fits is shown in Figs. 12 and 13, for alloys

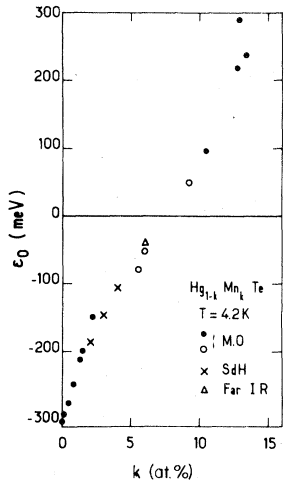

FIG. 10. Interaction gap ϵ_0 as a function of the Mn content. The dots for positive values of ϵ_0 are from the present work. The dots for $\epsilon_0 < 0$ are from magneto-optical measurements of Ref. 2. The crosses are from Shubnikov–deHaas measurements of Ref. 6. The triangle is from far-infrared measurements of S. W. McKnight, P. M. Amirtharaj, and S. Perkowitz, Solid State Commun. 25, 357 (1978).

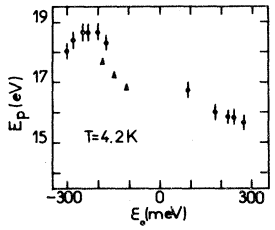

FIG. 11. The dependence of the matrix element E_p on the interaction gap ϵ_0. The circles are obtained from the present work and, for $\epsilon_0 < 0$, from magneto-optical data of Ref. 2. Vertical bars indicate margin of error. The triangles are from Ref. 6.

of various Mn content. Positive-gap ($k > 8$ at. %) alloys are characterized by a weak temperature dependence of the magnetization which slightly increases between 4.2 and 2 K, and also by a nearly linear field dependence of $A(H)$, as shown in Fig. 12.

The magnitude of $A(H,T)$ is by itself revealing. As can be seen from Fig. 13, which also includes previously published data[2] for low values of k for comparison, $A(H,T)$ is smaller for $k = 12.4$ at. % than for $k = 1.5$ at. %. All these features point out pronounced antiferromagnetic interactions between the localized magnetic moments. These interactions may have a short-range (superexchange) character or may be long range in nature due to the virtual electronic transitions across the small band gap separating the s and p levels (Bloembergen and Rowland mechanism). The long-range interaction has been evaluated for $Hg_{1-k}Mn_kTe$ alloys[12] and was shown to be antiferromagnetic, like the superexchange interaction. Both mechanisms should be taken into account to consistently describe the magnetization of $Hg_{1-k}Mn_kTe$ alloys. At a given temperature T a particular localized spin may be either frozen in an antiferromagnetically bound cluster so

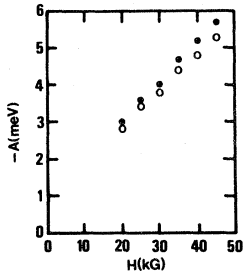

FIG. 12. Relative magnetization $A(H,T)$ as a function of the magnetic field at $T = 4.2$ (open circles) and 2 K (full circles) for an alloy of $k \simeq 12.8$ at. % ($\epsilon_0 = 219$ meV).

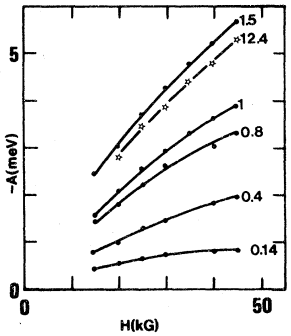

FIG. 13. Relative magnetization A as a function of magnetic field at $T = 4.2$ K for $Hg_{1-k}Mn_kTe$ alloys of different composition. The Mn content k (in at. %) is indicated for each curve. The stars correspond to the present work for the alloy with $k = 12.4$ at. %. The dots represent results for zero-gap $Hg_{1-k}Mn_kTe$, Ref. 2, shown for comparison. The solid curves for zero-gap materials are theoretical fits from Ref. 14. The solid line for the $k = 12.4$ at. % alloy is a guide for the eyes.

that it becomes ineffective, or, for more isolated spins, it may react to the external field with an effective temperature T_{eff} larger than T [see Eq. (9)] due to the long-range interaction between spins. Note that T_{eff} depends on T, as indicated by the downward bending of the inverse magnetic susceptibility, $\chi^{-1}(T)$, at low temperatures.[13,14] For very dilute alloys it was possible to account for the behavior of $\chi^{-1}(T)$ by assuming a long-range interaction between Mn^{2+} moments and considering only isolated spins and pairs.[15] In the present case, the $Hg_{1-k}Mn_kTe$ alloys are relatively concentrated, so that Mn ion pairs, triplets, and larger clusters have to be considered in the evaluation of $\chi(T)$. We have not attempted to calculate the magnetization of $Hg_{1-k}Mn_kTe$ alloys in this positive-gap composition range. Let us only remark that the curves $A(H)$ shown in Fig. 12, if considered as a function of $H/(T + T_{\text{eff}})$, would correspond to $T_{\text{eff}} \sim 25$ K. This value is consistent with the low-temperature behavior of $\chi^{-1}(T)$ reported by Nagata *et al.*[14] on $Hg_{1-k}Mn_kTe$ alloys of $k = 11$ at. % and $k = 14$ at. %.

E. Effect of exchange on Γ_6 and Γ_8 Landau levels

We present in Figs. 14 and 15 the magnetic field dependence of the first several Landau levels at $k_z = 0$ in the conduction and valence bands, respectively, for an alloy of $\epsilon_0 = 219$ meV. Two important features originating from the magnetic exchange

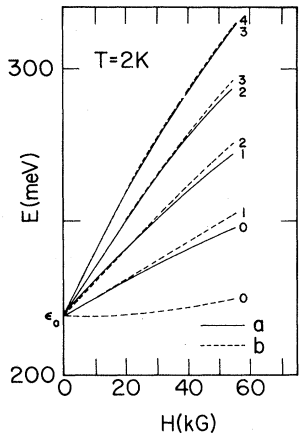

FIG. 14. Magnetic field dependence of Landau levels for conduction electrons (Γ_6 band) at $k_z = 0$ for an alloy with $\epsilon_0 = 219$ meV at $T = 2$ K, calculated using the modified Pidgeon-Brown model with the band and exchange parameters obtained from the present study.

interaction are illustrated in these figures:

1. The large exchange-induced shift of $b_{\Gamma_8}(-1)$ (i.e., the uppermost Landau level of the valence band) leads to a reduction of the energy gap in an applied magnetic field. The lowest-energy transition, $b_{\Gamma_8}(-1) \rightarrow b_{\Gamma_6}(0)$, allowed for the σ^- polarization, corresponds therefore to a *decreasing* photon energy as the magnetic field is increased. This effect occurs in alloys with energy gaps exceeding 180 meV.

2. In the conduction band, the relative positions of the spin sublevels $a_{\Gamma_6}(n)$ and $b_{\Gamma_6}(n)$ corresponding, respectively, to "spin-up" $(n\uparrow)$ and "spin-down" $(n\downarrow)$ electronic states, are inverted with respect to the usual ordering in zinc-blende semiconductors so that in the present case $E_a(n) > E_b(n)$. This important and new effect is a direct consequence of the s-d exchange interaction which shifts the spin sub-levels as shown in Fig. 16 [upwards for $a(n)$ and downwards for $b(n)$]. Thus, in the positive-gap semimagnetic alloys investigated here, the gyromagnetic factor of conduction electrons is *positive*. This is in complete contrast to zero-gap $Hg_{1-k}Mn_kTe$ and to nonmagnetic narrow-gap semiconductors such as InSb or $Hg_{1-x}Cd_xTe$, where the electronic g factors are always negative. The origin of the sign reversal of the g-factor occurring in materials under present study can be understood by expressing the spin sublevels of the nth Landau level in the Γ_6 band in the parabolic limit:

$$E_a(n) = (n + \tfrac{1}{2})\hbar\omega_c + \tfrac{1}{2}g_c^*\mu_B H - \tfrac{5}{4}\alpha k N_0 f_{\text{norm}} , \quad (14)$$

$$E_b(n) = (n + \tfrac{1}{2})\hbar\omega_c - \tfrac{1}{2}g_c^*\mu_b H + \tfrac{5}{4}\alpha k N_0 f_{\text{norm}} , \quad (15)$$

where ω_c is the cyclotron frequency, g_c^* is the g-factor determined by band structure alone (i.e., originating from the unmodified part of the Pidgeon-

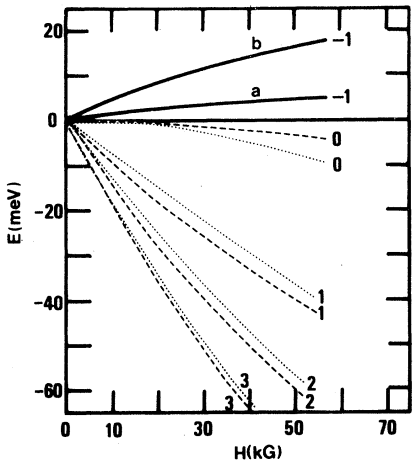

FIG. 15. Magnetic field dependence of Landau levels for the Γ_8 band at $k_z = 0$ for an alloy with $\epsilon_0 = 219$ meV at $T = 2$ K, calculated as in Fig. 14. Dashed lines represent light-hole levels corresponding to set a; dotted lines are for light-hole levels for set b. Solid lines show the $a(-1)$ and $b(-1)$ levels for heavy holes, as marked. Heavy-hole levels for $n \geq 1$ are not given, since they are very closely spaced and cannot be shown on the same scale.

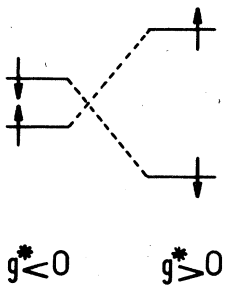

FIG. 16. Schematic illustration of the effect of exchange interaction on spin sublevels. Spin-up and spin-down levels correspond to the a and b sets, respectively. Spin sublevels without the exchange effect are shown on the left, representing the "normal" situation $[E(n\uparrow) < E(n\downarrow), g^* < 0]$. The exchange effect pushes $E(n\uparrow)$ upwards and $E(n\downarrow)$ downwards, reversing their order and resulting in a positive g^*, as shown on the right.

Brown model), and the last term is the s-d exchange contribution to the energy. Combining the exchange and the g_c^* terms, we can express the total spin splitting of the nth Landau level by means of an *effective* gyromagnetic factor[16]

$$\overline{g}^*_{\Gamma_6} = g_c^* - \frac{5}{2}\alpha\frac{kN_0}{\mu_B H} f_{\text{norm}}(H,T), \quad \alpha < 0 \ . \tag{16}$$

In narrow-gap semiconductors, g_c^* is negative. The exchange integral α for the Γ_6 band has also been shown to be negative, both in Ref. (2) and by the present results. One may therefore expect that, with increasing magnitude of the exchange interaction, the gyromagnetic factor for Γ_6 electrons will go through zero and subsequently reverse sign as the last term in Eq. (16) becomes dominant. Large and *positive* conduction-electron g factors are thus possible in open-gap semimagnetic semiconductors; e.g., for $\epsilon_0 = 219$ meV, we obtain $\overline{g}^*_{\Gamma_6} \approx 100$ at $H = 20$ kG. Note that in these materials the electron spin splitting can become comparable to the cyclotron energy, as can be seen in Fig. 14.

The same effect also exists in the light-hole Γ_8 band, as shown in Fig. 15. The relative positions of $a_l(n)$ and $b_l(n)$ ladders are again inverted with respect to the normal ordering, leading to positive light-hole g-factors which, however, are smaller than for conduction electrons.

ACKNOWLEDGMENTS

This work was supported by a contract of the D.G.R.S.T. (France). Two of us (J.K.F. and D.P.M.) would also like to thank the National Science Foundation (U.S.A.) for support through Grants No. DMR 77-23798 and DMR 79-23310.

*Laboratorie associé au Centre National de la Recherche † Scientifique.
† Present address: Naval Ocean Systems Center, San Diego, Calif. 92152.

[1]J. A. Gaj, R. Planel, and G. Fishman, Solid State Commun. 29, 435 (1979); J. A. Gaj, J. Ginter, and R. R. Galazka, Phys. Status Solidi B 89, 655 (1978).
[2]G. Bastard, C. Rigaux, Y. Guldner, J. Mycielski, and A. Mycielski, J. Phys. (Paris) 39, 87 (1978).
[3]C. Rigaux, G. Bastard, Y. Guldner, G. Rebmann, A. Mycielski, J. K. Furdyna, and D. P. Mullin, *Proceedings of the XV International Conference on Semiconductors, Kyoto, 1980,* J. Phys. Soc. Jpn. 49, Suppl. A, 811 (1980).
[4]M. Dobrowolska, W. Dobrowolski, M. Otto, T. Dietl, and R. R. Galazka, *Proceedings of the XV International Conference on Semiconductors, Kyoto, 1980,* J. Phys. Soc. Jpn. 49, Suppl. A, 815 (1980).
[5]Y. Guldner, C. Rigaux, M. Menant, D. P. Mullin, and J. K. Furdyna, Solid State Commun. 33, 133 (1980).
[6]Y. M. Jaczynski, J. Kossut, and R. R. Galazka, Phys. Status Solidi B 88, 73 (1978).
[7]C. R. Pidgeon and R. N. Brown, Phys. Rev. 146, 575 (1966).
[8]Y. Guldner, C. Rigaux, A. Mycielski and Y. Couder, Phys. Status Solidi B 81, 615 (1977); 82, 149 (1977).
[9]C. Rigaux (unpublished).
[10]J. Mycielski and C. Rigaux (unpublished).
[11]M. H. Weiler, R. L. Aggarwal, and B. Lax, Phys. Rev. B 16, 3603 (1977).
[12]C. Lewiner, J. A. Gaj, and G. Bastard, J. Phys. (Paris) Suppl. 41, C5-289 (1980).
[13]See, e.g., H. Savage, J. J. Rhyne, R. Holm, J. R. Cullen, C. E. Carroll, and E. P. Wohlfarth, Phys. Status Solidi B 58, 685 (1973).
[14]S. Nagata, R. R. Galazka, D. P. Mullin, H. Akbarzadeh, G. D. Khattak, J. K. Furdyna, and P. H. Keesom, Phys. Rev. B 22, 3331 (1980).
[15]G. Bastard and C. Lewiner, J. Phys. C 13, 1469 (1980).
[16]See, e.g., C. Rigaux, in *Narrow Gap Semiconductors: Physics and Applications,* Lecture Notes in Physics Series, No. 133 (Springer, Berlin, 1980), p. 110.